Chaotic Modeling and Simulation (CMSIM) 3: 295-304, 2018

A perturbed nonlinear model of an articulated vehicle with driver control

Zhaoheng Liu,[1] Kwok-wai Chung,[2] Wei Wang[3]

[1] Department of Mechanical Engineering, École de technologie supérieure, Université du Québec, 1100, Notre-Dame West Street, Montréal, Québec, Canada H3C 1K3
(E-mail: zhaoheng.liu@etsmtl.ca)

[2] Department of Mathematics, City University of Hong Kong, 83 Tat Chee Ave, Kowloon Tong, Hong Kong
(E-mail: makchung@cityu.edu.hk)

[3] School of Mechanical Engineering and Automation, Beihang University, Beijing, China
(E-mail: jwwx@163.com)

Abstract. A tractor-semitrailer is modeled by a multi-body system to study its planar motion for tracking maneuvers. In the model, driver steering control is also considered in a closed driver-vehicle system. The inherent parameters of the driver model are determined by an optimization algorithm. The resulting system is a 6-dimensional set of first-order nonlinear time-delayed differential equations. The linear stability boundaries are computed by a numerical root-finding algorithm to locate the right-most eigenvalues in the complex plane. Different nonlinear motions are found in the system in the vicinity of the bifurcation points using numerical simulations. When a periodic perturbation to the steering angle is considered, chaotic motions are observed. The influence on system behavior of such parameters as vehicle forward speed, and perturbation frequency and amplitude are studied.

Keywords: Chaotic motion, Tractor-semitrailer, Driver model, Time delay, Optimal control, Eigenvalues, Bifurcation and Simulation.

1 Introduction

Dynamic analysis of ground vehicles through modeling and simulation play an important role not only for vehicle design and optimization but also for improving road safety. There have been many research works on vehicle dynamics using different numbers of degrees of freedom (DOF) to model vehicles, depending on the purpose of the study [1-2]. For handling and stability analyses, only lateral and yaw motions are usually considered [3-6]. In this paper, a tractor-semitrailer is modeled by a 3-DOF system to study its planar motion for tracking maneuvers [3-4]. Driver steering control is also factored into the model. The vehicle is supposed to move on a horizontal plane in a straight line at a constant forward speed. The driver takes steering action when the vehicle's path deviates from the desired centerline. The parameters in the driver model are determined using a previously developed algorithm [4]. The

Received: 26 October 2017 / Accepted: 23 March 2018

ISSN 2241-0503

resulting closed-loop dynamic system contains a time delay representing the driver's inherent physiological response time. In the following sections, after a short summary of the dynamic equations of the system from [3], simulation results are presented. The nonlinear non-autonomous system can exhibit qualitatively different behaviors, such as asymptotically stable, single-frequency oscillations, and subharmonic and chaotic motion. It is seen that disturbance amplitude and frequency are important factors that affect the type of nonlinear vehicle behavior.

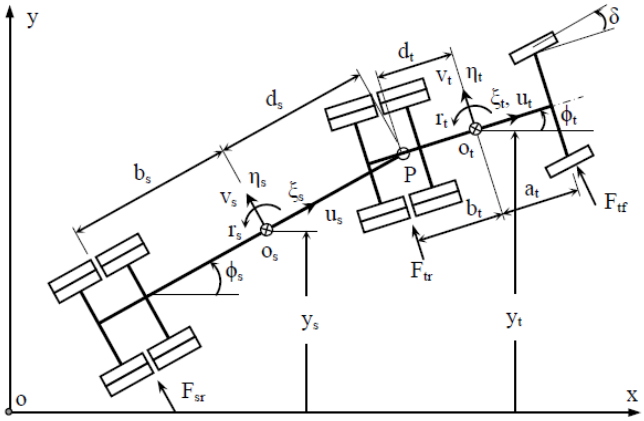

Fig. 1. 3-DOF vehicle model [3]

2 Nonlinear time-delayed system equations

The 3-DOF vehicle model is presented in Fig. 1. As developed in [3], the planar motion of the tractor-semitrailer is governed by the following equations:

$$\begin{aligned} m_t(\dot{v}_t + ur_t) &= 2F_{tf} + 8F_{tr} + F_{P\eta t} \\ I_{zt}\dot{r}_t &= 2a_tF_{tf} - 8b_tF_{tr} - d_tF_{P\eta t} \\ m_s(\dot{v}_s + ur_s) &= 8F_{sr} + F_{P\eta s} \\ I_{zs}\dot{r}_s &= -8b_sF_{sr} + d_sF_{P\eta s} \end{aligned} \tag{1}$$

The equations above are established using Newton's law in the local body-fixed coordinate systems ($O_t\xi_t\eta_t$) and ($O_s\xi_s\eta_s$) for the tractor and semitrailer units respectively. The lateral forces developed at the tire-ground contact are modeled as a cubic function of side-slip angles:

$$\begin{aligned} F_{tf} &= -(C_{tf}\alpha_{tf} - C_{tf3}\alpha_{tf}^3) \\ F_{tr} &= -(C_{tr}\alpha_{tr} - C_{tr3}\alpha_{tr}^3) \\ F_{sr} &= -(C_{sr}\alpha_{sr} - C_{sr3}\alpha_{sr}^3) \end{aligned} \tag{2}$$

In (2), the side-slip angles are defined as:

$$\begin{aligned} \alpha_{tf} &= arctan\left(\frac{v_t + a_t r_t}{u}\right) - \delta(t) \\ \alpha_{tr} &= arctan\left(\frac{v_t - b_t r_t}{u}\right) \\ \alpha_{sr} &= arctan\left(\frac{v_s - b_s r_s}{u}\right) \end{aligned} \tag{3}$$

where $\delta(t)$ represents the front steering angle of the tractor:

$$\delta(t) = \bar{\delta}(t) + \delta_d(t) = \bar{\delta}(t) + Qcos(\omega_d t) \tag{4}$$

In this work, not only the steering angle $\bar{\delta}(t)$ produced by the driver is considered, but also a sinusoidal disturbance $\delta_d(t)$ due to road irregularities with frequency $\omega_d = 2\pi u/L_d$, where u is the vehicle's forward speed and L_d is the wavelength of road irregularities.

As described in [3], driver steering control is modeled as feedback to vehicle lateral and heading states with a time delay τ:

$$\begin{aligned} \bar{\delta}(t) = {} & h_4 y_t(t-\tau) + h_5\phi_t(t-\tau) + h_6\phi_s(t-\tau) \\ & + h_1\dot{y}_t(t-\tau) + h_2\dot{\phi}_t(t-\tau) + h_3\dot{\phi}_s(t-\tau) \end{aligned} \tag{5}$$

Tractor and semitrailer lateral displacements $y_t(t)$ and $y_s(t)$ and heading angles $\phi_t(t)$ and $\phi_s(t)$ are expressed in the fixed coordinate system. They are related to the body-fixed coordinate variables (v_t, r_t, v_s, r_s) as follows:

$$\begin{aligned} \dot{\phi}_t &= r_t \\ \dot{y}_t &= v_t\, cos(\phi_t) + u_t\, sin(\phi_t) = v_t + u\phi_t \\ \dot{\phi}_s &= r_s \\ \dot{y}_s &= v_s\, cos(\phi_s) + u_s\, sin(\phi_s) = v_s + u\phi_s \end{aligned} \tag{6}$$

Define the system state variable vector as:

$$x(t) = \left(y_t(t), \phi_t(t), \phi_s(t), \dot{y}_t(t), \dot{\phi}_t(t), \dot{\phi}_s(t)\right)^T \in \mathbb{R}^6 \tag{7}$$

Using the variables defined in (7), the side-slip angles given in (3) can be expressed in terms of state variables as:

$$\begin{aligned}
\alpha_{tf} &= arctan\left(\frac{a_t x_5(t) - u x_2(t) + x_4(t)}{u}\right) - \left(h_4 x_1(t-\tau) + h_5 x_2(t-\tau) + h_6 x_3(t-\tau)\right. \\
&\quad \left. + h_1 x_4(t-\tau) + h_2 x_5(t-\tau) + h_3 x_6(t-\tau) + Qcos(\omega_d t)\right) \\
\alpha_{tr} &= arctan\left(\frac{-b_t x_5(t) - u x_2(t) + x_4(t)}{u}\right) \\
\alpha_{sr} &= arctan\left(\frac{-b_s x_6(t) + u(x_2(t) - x_3(t)) - u x_2(t) + x_4(t) - d_t x_5(t) - d_s x_6(t)}{u}\right)
\end{aligned} \tag{8}$$

It is noted that action and reaction forces $F_{p\eta t}$ and $F_{p\eta s}$ at the articulation point can be considered of the same magnitude with opposite signs, assuming a small angle between the tractor and semitrailer. One equation can thus be eliminated from (1). The motion of the 3-DOF multi-body system can then be described by a 6-dimensional nonlinear dynamic equation using the state vector defined in (7) as:

$$\dot{x}(t) = f(x(t), x(t-\tau), t, \gamma) \tag{9}$$

where

$$\begin{aligned}
f_1 &= x_4 \\
f_2 &= x_5 \\
f_3 &= x_6 \\
f_4 &= 2\left(-4F_{sr} I_{zt} b_s d_s m_s + \left(F_{tf} I_{zs} a_t + F_{tf} I_{zs} d_t - 4F_{tr} I_{zs} b_t\right) d_t m_s\right. \\
&\quad + 4F_{tr}\left(I_{zs} d_t^{\,2} + I_{zt} d_s^{\,2}\right) m_s + \left(4F_{sr} + F_{tf} + 4F_{tr}\right) I_{zs} I_{zt}\Big) / \\
&\quad \left(\left(I_{zs} d_t^{\,2} + I_{zt} d_s^{\,2}\right) m_s m_t + I_{zs} I_{zt}\left(m_s + m_t\right)\right) \\
f_5 &= -2\left(\left(-4F_{sr} b_s d_t - F_{tf} a_t d_s + 4F_{tr} b_t d_s\right) d_s m_s m_t + 4F_{sr} I_{zs} d_t m_t\right. \\
&\quad \left. - F_{tf} I_{zs}\left(a_t m_s + a_t m_t - d_t m_s\right) + 4F_{tr} I_{zs}\left(b_t m_s + b_t m_t - d_t m_s\right)\right) / \\
&\quad \left(\left(I_{zs} d_t^{\,2} + I_{zt} d_s^{\,2}\right) m_s m_t + I_{zs} I_{zt}\left(m_s + m_t\right)\right) \\
f_6 &= -2\left(\left(4F_{sr} b_s d_t + F_{tf} a_t d_s - 4F_{tr} b_t d_s\right) d_t m_s m_t\right. \\
&\quad \left. + 4F_{sr} I_{zt}\left(b_s m_s + b_s m_t + d_s m_t\right) - \left(F_{tf} + 4F_{tr}\right) I_{zt} d_s m_s\right) / \\
&\quad \left(\left(I_{zs} d_t^{\,2} + I_{zt} d_s^{\,2}\right) m_s m_t + I_{zs} I_{zt}\left(m_s + m_t\right)\right)
\end{aligned}$$

The last three functions are expressed in terms of state variables through (2) and (8).

3 Simulation results

3.1 Stability of the autonomous system (Q = 0)

When disturbance $\delta_d(t)$ in (4) is ignored, the system (9) becomes autonomous. In this case, it is possible to linearize this time-delayed system and compute its eigenvalues using a numerical algorithm presented in [4, 5]. A nonlinear analysis can also be conducted using an integration method [3]. To illustrate different behaviors, the parameter values below will be used for a stability analysis of the closed-loop system.

Common vehicle and driver parameters (same as in [3]) are as follows:

m_t = 8,444 kg	m_s = 23,472 kg	I_{zt} = 65,735 kg·m^2
I_{zs} = 181,565 kg·m^2	a_t = 2.59 m	b_t = 3.29 m
d_t = 3.06 m	d_s = 4.2 m	b_s = 9.65 – d_s
h_1 = -0.127422	h_2 = -0.174386	h_3 = -0.054087
h_4 = -0.045962	h_5 = -0.006909	h_6 = 0.033233
τ = 0.2 s		

As a first example (**Case 1**), the common parameters above are accompanied by the following tire cornering parameters:

C_{tf1} = 143,330.0 N/rad	C_{tr1} = 143,330.0 N/rad	C_{sr1} = 80,312.0 N/rad
C_{tf3} = 553,740.0 N/rad^3	C_{tr3} = 553,740.0 N/rad^3	C_{sr3} = 350,590.0 N/rad^3

For Case 1, using the numerical root-locating method based on labeling a bounded region in the complex plane [4, 5], a critical forward speed (u_c) can be determined such that a pair of conjugate eigenvalues is located on the imaginary axis and all other eigenvalues are to the left of that axis. The critical speed is found to be u_c = 53.816 m/s and the imaginary part of the eigenvalues are ±5.01359, which corresponds to the critical frequency ω_c = 5.01359 rad/s. A further nonlinear analysis conducted in [3] concluded that this is a case of supercritical Hopf bifurcation.

As a second example (**Case 2**), the same common parameters are accompanied by following the tire cornering parameters:

C_{tf1} = 80,312.0 N/rad	C_{tr1} = 80,312.0 N/rad	C_{sr1} = 143,330.0 N/rad
C_{tf3} = 350,590.0 N/rad^3	C_{tr3} = 350,590.0 N/rad^3	C_{sr3} = 553,740.0 N/rad^3

Case 2 results in subcritical bifurcation, critical speed u_c = 35.179 m/s and critical frequency ω_c = 2.38266 rad/s [3].

3.2 System simulation with disturbance $\delta_d = Q\cos(\omega_d t)$

Applying a harmonic disturbance to the front wheels, as described in (4), vehicle behavior in the vicinity of bifurcation points is investigated when such a

disturbance occurs for cases of supercritical bifurcation (Case 1). Recall for supercritical bifurcation that, in the absence of the disturbance, system motion converges to the equilibrium point before reaching the critical parameter value; whereas, the system undergoes a stable limit cycle motion after passing the bifurcation point. It is of interest to examine the system's behavior in the presence of a disturbance.

Consider a disturbance with Q = 0.0524 rad and $\omega_d = \omega_c/2$ for the parameter values in Case 1. The simulation results are shown in Fig. 2 and Fig. 3 for forward speed $u = u_c + 3$ m/s, which is beyond its critical value. The phase diagram and a fast Fourier transform (FFT) of the time-history signal show that the vehicle's motion is subharmonic with ω_d being the base frequency.

Using the same disturbance parameters and taking a forward speed lower than its critical value, $u = u_c - 3$ m/s, yields the simulation results presented in Fig. 4 and Fig. 5. Due to the effect of this disturbance, the asymptotical stable motion becomes oscillatory. As can be seen from Fig. 5, the oscillation has only one frequency component, which is the excitation frequency ω_d.

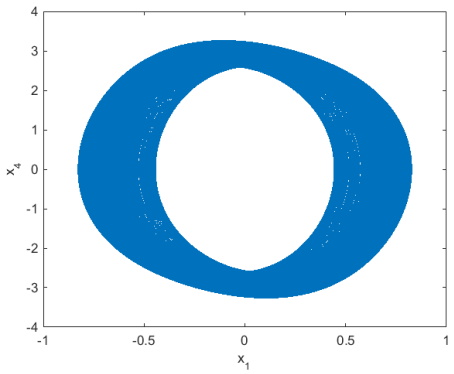

Fig. 2. Phase diagram for Q = 0.0524 rad, $\omega_d = \omega_c/2$ and $u = u_c + 3$ m/s

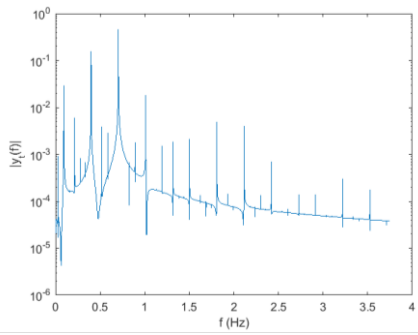

Fig. 3. FFT for Q = 0.0524 rad, $\omega_d = \omega_c/2$ and $u = u_c + 3$ m/s

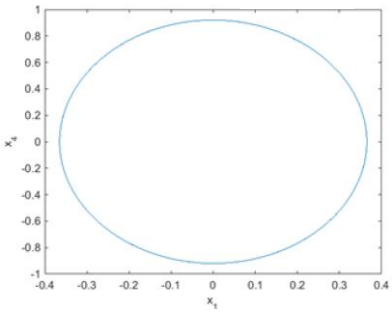

Fig. 4. Phase diagram for Q = 0.0524 rad, $\omega_d = \omega_c/2$ and $u = u_c - 3$ m/s

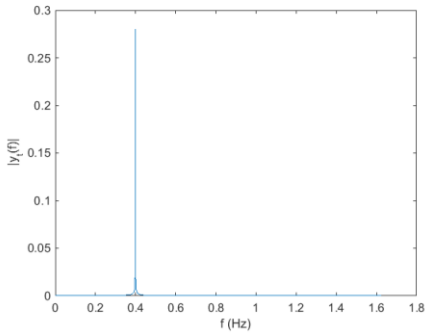

Fig. 5. FFT for Q = 0.0524 rad, $\omega_d = \omega_c/2$ and $u = u_c - 3$ m/s

A bifurcation diagram can be drawn for a broad view of the system's behavior over a range of forward speeds. Assuming a road disturbance wavelength of L_d, frequency ω_d is expressed as $\omega_d = 2\pi u/L_d$. Fig. 6 presents a bifurcation diagram using L_d = *45* m. To draw this diagram, for a given value of u, a simulation is run for t = *0* to t_f with a time step Δt using the fourth-order Runge-Kutta method. Then, state variable $y_t(t)$ is sampled using frequency ω_d (its period $T_d = 2\pi/\omega_d$) and the points are plotted as $[u, y_t(t_0+i\cdot T_d)]$, where $i = 1 \ldots N$ in the diagram. From the diagram shown in Fig. 6, different behaviors of the system can be observed. For instance, for $u < u_c + \varepsilon \approx 55$ m/s, where ε is a positive real number, the system undergoes a simple harmonic motion with only one frequency ω_d, i.e., all N points are superimposed to one point for a given value of u in the diagram. As the forward speed increased beyond $u_c + \varepsilon$, the motion contains multiple discrete frequency components. Careful examination shows that the transition at $u = u_c + \varepsilon$ is from a simple harmonic motion to a subharmonic or quasi-periodic motion. It is also interesting to note that there is a small window around u = 64 m/s in which a frequency-locking phenomenon with period-2 motion appears, i.e., there are only two separate points for a given value of u for a small range of u. However, no chaotic motion

appears within this set of disturbance and driving parameters over the entire range of $u \in$ [50 67] in this diagram.

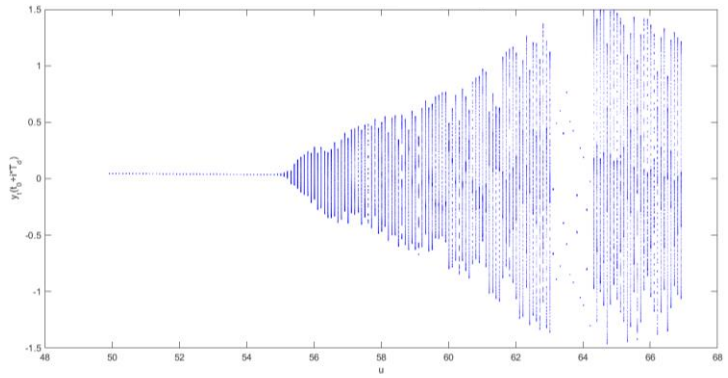

Fig. 6. Bifurcation diagram for Q = 0.05 rad and $\omega_d = 2\pi u/L_d$

A set of extreme parameters values is now taken to demonstrate the existence of chaotic motion. The disturbance frequency is set to ω_d = 0.2 ω_c and the forward speed to u = u_c + 10 m/s for Case 1. When the disturbance amplitude is increased and reaches a critical value, the system exhibits chaotic motion, as shown in Fig. 7, Fig. 8 and Fig. 9. The chaotic behavior is first seen in the phase diagram (Fig. 7), in which the trajectory on plane x_1-x_4 tends to fill a certain area without repetition. One important characteristic of chaotic motion is the continuous frequency spectrum of its time series. As shown in Fig. 8, no discrete frequency components appear in the FFT of $y_t(t)$, the spectrum being rather continuous. The Poincaré map obtained using sampling frequency ω_d (Fig. 9) also confirms the chaotic nature of the motion since certain areas are densely filled with intersection points. Another mathematical tool for determining chaos is the Lyapunov exponents [7, 8]. In [9], chaotic motion was successfully confirmed by positive Lyapunov exponents over a certain range of the bifurcation parameter. Due to the complexity of the dynamic equation under study and the time delay in the model, Lyapunov exponents for the system have not yet been computed. This may be a useful area of future study.

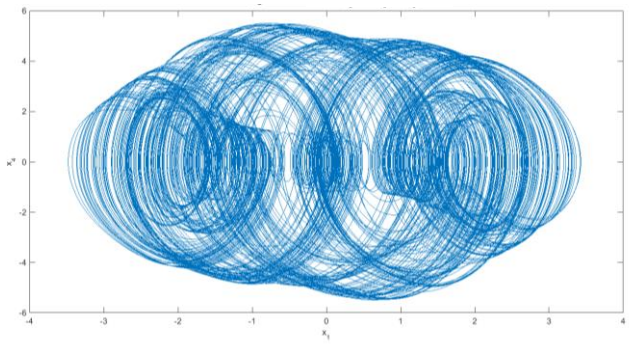

Fig. 7. Phase diagram for Q = 0.233 rad, ω_d = 0.2 ω_c and u = u_c + 10 m/s

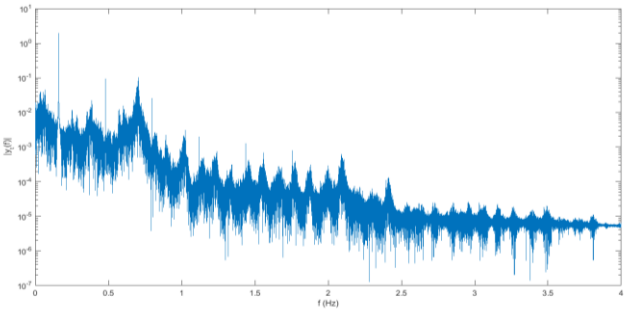

Fig. 8. FFT for Q = 0.233 rad, ω_d = 0.2 ω_c and u = u_c + 10 m/s

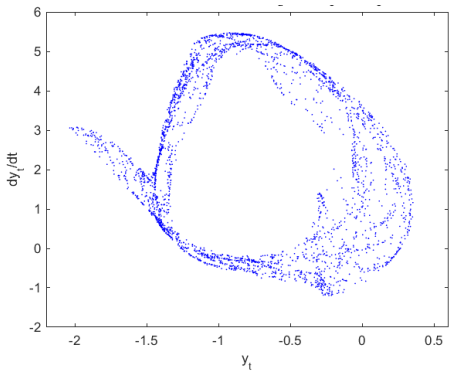

Fig. 9. Poincaré map for Q = 0.233 rad, ω_d = 0.2 ω_c and u = u_c + 10 m/s

Conclusions

In this paper, a nonlinear non-autonomous time-delayed system of an articulated vehicle with driver steering control is studied using numerical simulations. With disturbances to the front wheels, it is found that the vehicle system exhibits qualitatively different behaviors, such as simple oscillations, subharmonic

motion and chaotic motion. From the results obtained in this study, it is interesting to note that the vehicle's motion may contain very rich frequency components with bounded amplitude. Even though chaotic motion is found in a small area of parameter values, the amplitude and frequency of the disturbance go beyond their realistic values.

References

1. M. Gäfvert, O. Lindgärde, A 9-DOF tractor-semitrailer dynamic handling model for advanced chassis control studies, *Vehicle System Dynamics* **41**(1), 51–82, 2004.
2. C. Cheng, R. Roebuck, A. Odhams, D. Cebon, High-speed optimal steering of a tractor–semitrailer, *Vehicle System Dynamics* **49**(4), 561–593, 2011.
3. Z. Liu, K. Hu, K.-w. Chung, Nonlinear analysis of a closed-loop tractor-semitrailer vehicle system with time delay, *Mechanical Systems and Signal Processing* **76-77**, 696–711, 2016.
4. Z. Liu, Characterisation of optimal human driver model and stability of a tractor-semitrailer vehicle system with time delay, *Mechanical Systems and Signal Processing* **21**, 2080–2098, 2007.
5. Z. Liu, G. Payre, P. Bourassa, Stability and nonlinear oscillations a in a time-delayed vehicle system with driver control, *Nonlinear Dynamics* **35**, 159–173, 2004.
6. Z. Liu, G. Payre, Global bifurcation analysis of a nonlinear road vehicle system, *ASME Journal of Computational and Nonlinear Dynamics* **2**, 308–315, 2007.
7. A. Wolf, J. B. Swift, H. L. Swinney, J. A. Vastano, Determining Lyapunov exponents from a time series, *Physica* **6D**, 285–317, 1985.
8. F. C. Moon, *Chaotic and Fractal Dynamics*, John Wiley & Sons, New York, 1992.
9. Z. Liu, G. Payre, P. Bourassa, Nonlinear oscillations and chaotic motions in a road vehicle system with driver steering control, *Nonlinear Dynamics* **9**, 281–304, 1996.